Size and Rigidity of Cylindrical Polymer Brushes Dictate Long Circulating Properties *In Vivo*

Markus Müllner,[†,§,⊥] Sarah J. Dodds,[†,§,⊥] Tri-Hung Nguyen,[‡,§] Danielle Senyschyn,[‡,§] Christopher J. H. Porter,[*,‡,§] Ben J. Boyd,[*,‡,§] and Frank Caruso[*,†,§]

[†]Department of Chemical and Biomolecular Engineering, The University of Melbourne, Parkville, Victoria 3010, Australia, [‡]Drug Delivery Disposition and Dynamics, Monash Institute of Pharmaceutical Sciences, Monash University, Parkville, Victoria 3052, Australia, and [§]ARC Centre of Excellence in Convergent Bio-Nano Science and Technology. [⊥]M.M. and S.J.D. contributed equally.

ABSTRACT Studies of spherical nanoengineered drug delivery systems have suggested that particle size and mechanical properties are key determinants of *in vivo* behavior; however, for more complex structures, detailed analysis of correlations between *in vitro* characterization and *in vivo* disposition is lacking. Anisotropic materials in particular bear unknowns in terms of size tolerances for *in vivo* clearance and the impact of shape and rigidity. Herein, we employed cylindrical polymer brushes (CPBs) to answer questions related to the impact of size, length and rigidity on the *in vivo* behavior of PEGylated anisotropic structures, in particular their pharmacokinetics and biodistribution. The modular grafting assembly of CPBs allowed for the systematic tailoring of parameters such as aspect ratio or rigidity while keeping the overall chemical composition the same. CPBs with altered length were produced from polyinitiator backbones with different degrees of polymerization. The side chain grafts consisted of a random copolymer of poly[(ethylene glycol) methyl ether methacrylate] (PEGMA) and poly(glycidyl methacrylate) (PGMA), and rendered the CPBs water-soluble. The epoxy groups of PGMA were subsequently reacted with propargylamine to introduce alkyne groups, which in turn were used to attach radiolabels *via* copper(I)-catalyzed alkyne—azide cycloaddition (CuAAC). Radiolabeling allowed the pharmacokinetics of intravenously injected CPBs to be followed as well as their deposition into major organs post dosing to rats. To alter the rigidity of the CPBs, core—shell-structured CPBs with polycaprolactone (PCL) as a water-insoluble and crystalline core and PEGMA-*co*-PGMA as the hydrophilic shell were synthesized. This modular buildup of CPBs allowed their shape and rigidity to be altered, which in turn could be used to influence the *in vivo* circulation behavior of these anisotropic polymer particles. Increasing the aspect ratio or altering the rigidity of the CPBs led to reduced exposure, higher clearance rates, and increased mononuclear phagocytic system (MPS) organ deposition.

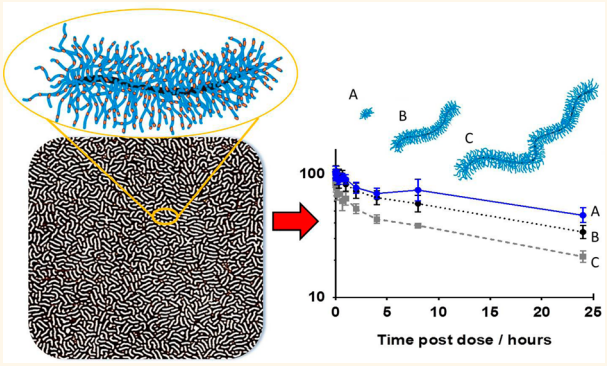

KEYWORDS: grafting-from · PEGylation · biodistribution · long circulation · pharmacokinetics · anisotropic polymer particles · macrophages

Molecular weight, polymeric architecture, interfacial properties and particle size have been well described as key drivers of the *in vivo* behavior of nanomaterials and have motivated many *in vitro*[1−5] and *in vivo* studies of nanoparticle properties.[6−13] The majority of these studies have focused on spherical systems; however, recently the focus has increasingly shifted toward anisotropic structures in order to establish the influence of shape and geometry of particulate carrier systems on their *in vivo* performance.[14−17] It has been shown that particle geometry influences interactions with cells and can alter the circulation of particles that may improve exposure and pharmacological effects. Although some nonspherical systems, including viruses,[18,19] silica or gold rods,[20,21] carbon nanotubes,[22−24] stretched polymer spheres[15] and PRINT particles[25,26] have been studied, showing *in vivo* half-lives ranging from minutes to several hours (~12 h), thus far there have only been a small number of reports on the *in vivo* behavior of anisotropic polymer particles. This is, in part, a result of challenges associated with the production of nonspherical

* Address correspondence to fcaruso@unimelb.edu.au, ben.boyd@monash.edu.au, chris.porter@monash.edu.

Received for review September 11, 2014 and accepted January 18, 2015.

Published online January 29, 2015
10.1021/nn505125f

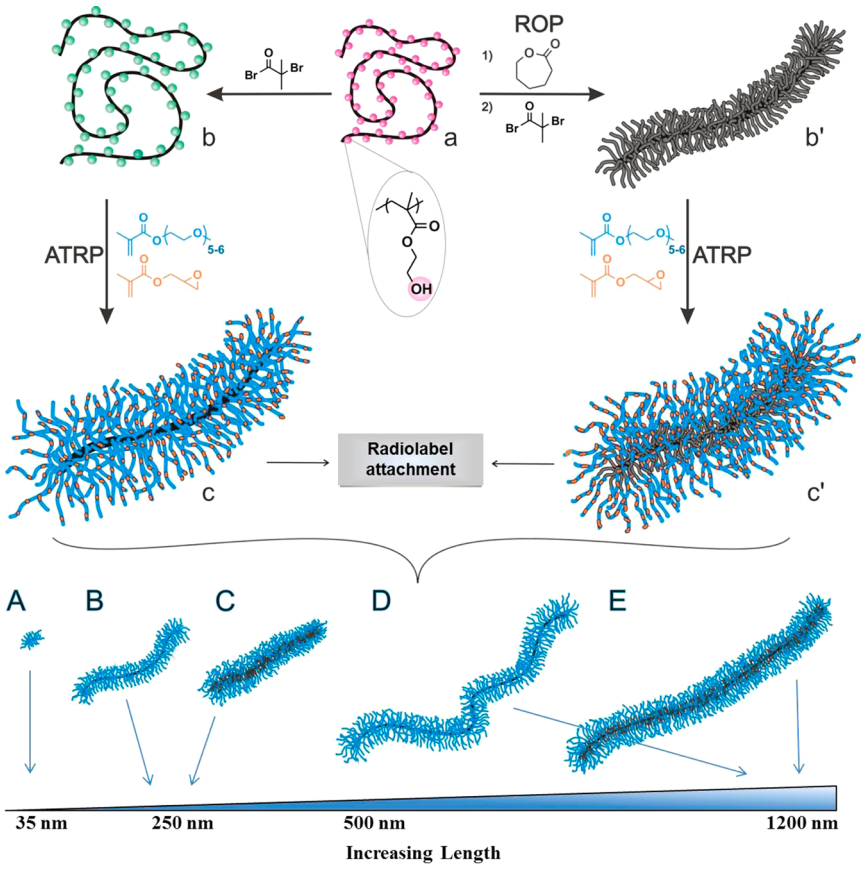

Scheme 1. PHEMA (a) is either modified to yield PBIEM (b) or PCL (b′). Subsequently, side chains are grafted *via* ATRP to from either epoxy-functionalized PEGMA (c) or epoxy-functionalized PCL−PEGMA core-shell CPBs (c′). A−E show the library of synthesized CPBs with different lengths.

particles with precise control over both morphology and physicochemical properties. In this regard, cylindrical polymer brushes (CPBs) provide new opportunities to better understand the relationships between size, shape, rigidity and *in vivo* behavior since they are essentially unimolecular polymers, but can be synthesized to exhibit particle-like dimensions. CPBs, sometimes referred to as molecular brushes, are anisotropic polymers that can be synthetically assembled *via* several established grafting strategies.[27,28] CPBs generally exhibit a polymer backbone that is grafted with polymer side chains. The use of controlled polymerization techniques gives excellent control over the composition of the CPBs while also enabling the precise tailoring of their morphology, such as length and diameter. With increasing grafting density of the side chains, steric hindrance of the grafts forces the backbone to stretch, which in turn results in the characteristic cylindrical shape of CPBs. To date, only a small number of *in vitro* reports[29−32] have described potential biomedical applications of cylindrical polymer particles,[33] showing composition-dependent cellular interactions and strategies to release drugs to kill cancer cells. Recently, small PEG bottlebrushes have been assembled into larger PEG star polymers to deliver anticancer drugs *in vivo*.[34] However, CPBs have been largely overlooked in terms of their potential in biomedicine.[35] In particular, the *in vivo* pharmacokinetic behavior of these materials has not been described, despite previous studies revealing that worm-shaped cylindrical polymer micelles show extended circulation half-lives when compared to stealth polymersomes.[36,37]

Herein, we sought to investigate the *in vivo* behavior of CPBs and to evaluate the impact of changes to length and rigidity on *in vivo* clearance, distribution and persistence (half-life). To that end, a library of CPBs containing poly[(ethylene glycol) methyl ether methacrylate] (PEGMA) as the main structural component was synthesized (Scheme 1 and in Supporting Information S1). CPBs of this type have advantages over other anisotropic materials such as cylindrical micelles since they allow the generation of anisotropic polymer particles while maintaining good control over length distribution. Thus, CPBs can be produced with narrow length distributions and an overall length below 2 μm, a goal that remains challenging *via* self-assembly of block copolymers, despite efforts using crystallization[38,39] or extrusion.[38] PEG-based materials were employed in our study to impart a hydrophilic corona to the system, thereby reducing opsonization and avoiding rapid uptake by the mononuclear

phagocyte system (MPS). Small amounts of epoxy groups were incorporated into the PEGMA grafts to allow for postmodification reactions and, in this work, to facilitate stable conjugation with a tritiated aspirin analogue to allow quantification of *in vivo* pharmacokinetics. In order to alter the rigidity of the CPBs, we also integrated a hydrophobic core compartment into two of the CPB analogues. The current studies provide confirmation of long circulatory behavior for these materials and suggest that while increasing length and rigidity increases clearance by the major MPS organs (liver, spleen), CPBs with molecular weights as high as 500 000 000 $g \cdot mol^{-1}$ still provide for high longevity *in vivo* with terminal half-lives of greater than 20 h. Spherical PEGylated dendrimers may achieve higher terminal half-lives *in vivo* (up to ~80 h), however, their molecular weights are far smaller (below 70 000 $g \cdot mol^{-1}$) than the studied CPBs.[40] Furthermore, the synthetic assembly of CPBs is useful for producing low-fouling materials that consist almost solely of PEG, which would not be possible *via* traditional self-assembly approaches. Hence, CPBs offer an interesting platform for the study of pharmacokinetics and biodistribution of cylindrical polymer objects, as their dimensions can be readily tailored by polymerization. Understanding the *in vivo* behavior of engineered particles, such as particle clearance and biodistribution, is a crucial step in establishing the potential usefulness of polymeric drug carriers.

RESULTS AND DISCUSSION

Synthesis of the Water-Soluble CPBs. As illustrated in Scheme 1 (and in the Supporting Information S1), we combined several polymerization techniques to obtain a library of CPBs with tailor-made characteristics. First, PHEMA was produced by the polymerization and subsequent deprotection of trimethylsilyl-protected HEMA (TMS-HEMA). Two different synthetic routes were used. For short PHEMA backbones (degree of polymerization (DP) ~100), it was sufficient to use controlled radical polymerization, in this case ATRP. However, for longer PHEMA backbones (DP > 1000), anionic polymerization was employed to obtain a high DP while maintaining sufficient control over the molecular weight distribution. Second, PHEMA (a) was either modified with an ATRP initiator (b), to give poly(2-(2-bromoisobutyryloxy)ethyl methacrylate) (PBIEM), or directly used as a polyinitiator backbone for the grafting of caprolactone. Polycarpolactone (PCL) homopolymer brushes (b′) were synthesized by ring-opening polymerization (ROP) in bulk using tin(II) 2-ethylhexanoate, $Sn(Oct)_2$ as a catalyst. The terminal groups of the PCL brush side chains are also hydroxyl groups, which were subsequently modified with an ATRP initiator. Finally, PEGMA, containing 15 mol % GMA, was grafted from both the PBIEM backbones (c) and the ATRP initiator-functionalized PCL brushes (c′), respectively. Consequently, several water-soluble CPBs with different lengths were obtained (Table 1).

TABLE 1. Overview of the Synthesized CPBs

	composition[a]	length (nm)	MW ($kg \cdot mol^{-1}$)
A	$[PEGMA_{140}\text{-}co\text{-}GMA_{21}]_{112}$	35[b]	5000
B	$[PEGMA_{188}\text{-}co\text{-}GMA_{32}]_{2700}$	220 ± 70[c]	164 000
C	$[PCL_{25}\text{-}b\text{-}(PEGMA_{98}\text{-}co\text{-}GMA_{16})]_{2700}$	260 ± 50[c]	412 000
D	$[PEGMA_{170}\text{-}co\text{-}GMA_{28}]_{7500}$	1150 ± 300[c]	93 000
E	$[PCL_{14}\text{-}b\text{-}(PEGMA_{94}\text{-}co\text{-}GMA_{16})]_{7500}$	1200 ± 200[c]	240 000

[a] Determined by ^1H NMR (calculated using 50% grafting efficiency from PBIEM and 90% grafting efficiency from PCL brush). [b] Number-weighted DLS (hydrodynamic diameter). [c] Average length determined from AFM.

^1H NMR measurements were used to follow each step of the polymer brush build-up. Each modification and grafting step can be found in the Supporting Information (S1). ^1H NMR of purified brush solutions revealed the successful copolymerization of GMA and PEGMA, and hence the incorporation of epoxy groups into the side chains (Figure 1). Glycidyl methacrylate containing polymers have been reported to be highly versatile for postfunctionalization.[41,42] Consequently, the CPBs were further treated with AF647 cadaverine dye to introduce fluorescent tags or reacted with propargylamine to modify some of the glycidyl methacrylate units with alkyne functionalities. IR measurements indicated the successful incorporation of alkyne groups into the polymer brushes (Supporting Information S2). These alkyne groups were then used to attach radiolabels (^3H 4-azidosalicylic acid) onto the CPBs *via* copper(I)-catalyzed alkyne−azide cycloaddition (CuAAC). Liquid scintillation counting was used to evaluate the attachment of the radiolabel to the modified brushes (Supporting Information S3).

Dynamic light scattering (DLS) was used to measure the hydrodynamic diameter of the shortest CPB, $[PEGMA_{140}\text{-}co\text{-}GMA_{21}]_{112}$. DLS revealed a diameter of 35 nm (see Supporting Information S4). Because of the similar DP of the backbone and the side chains, it was assumed that this CPB could be approximated to spherical in shape in solution, rather than the typical cylindrical shape of CPBs. DLS was found unsuitable for determination of the dimensions of the CPBs with longer backbones; therefore, atomic force microscopy (AFM) was used to establish the shape and lengths of the anisotropic CPBs (Figure 2). The similarity in side chain length of the CPBs lacking the PCL core suggests that their diameters are comparable. Additional cross section analyses and AFM phase images further confirmed the similarity in width of the CPBs on mica (see Supporting Information S5).

Table 1 gives an overview of the lengths of the CPBs measured by AFM. The main difference between the CPBs with the same backbone length is that one type

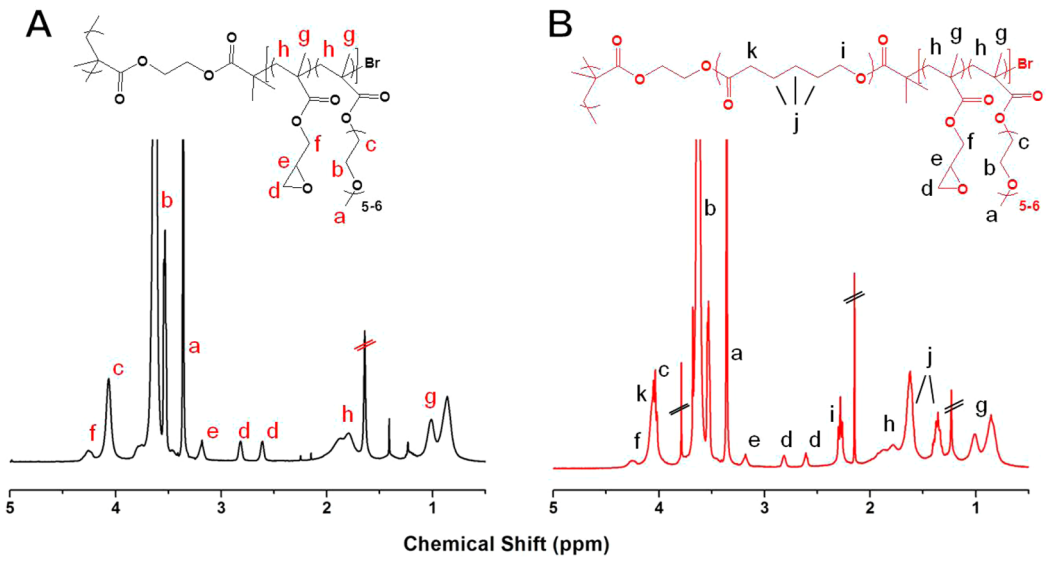

Figure 1. ^{1}H NMR spectra of (A) [PEGMA$_{140}$-*co*-GMA$_{21}$]$_{112}$ and (B) [PCL$_{25}$-*b*-(PEGMA$_{98}$-*co*-GMA$_{16}$)]$_{2700}$ in $CDCl_3$.

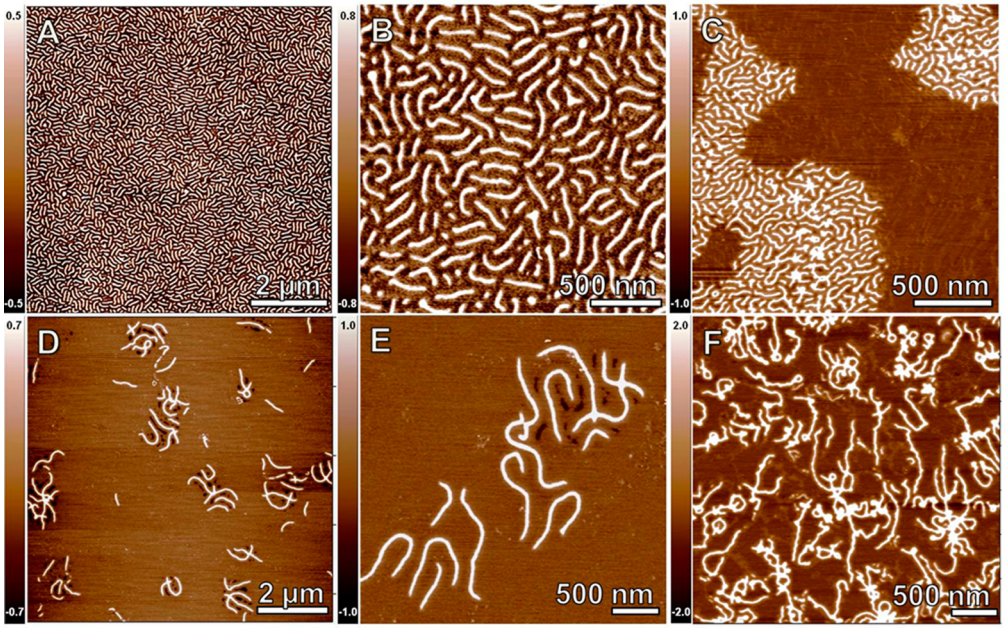

Figure 2. AFM height images of air-dried CPBs deposited from acetone on mica: (A,B) [PCL$_{25}$-*b*-(PEGMA$_{98}$-*co*-GMA$_{16}$)]$_{2700}$, (C) [PEGMA$_{188}$-*co*-GMA$_{32}$]$_{2700}$, (D,E) [PCL$_{14}$-*b*-(PEGMA$_{94}$-*co*-GMA$_{16}$)]$_{7500}$, and (F) [PEGMA$_{170}$-*co*-GMA$_{28}$]$_{7500}$, respectively.

of CPB was synthesized with a water-insoluble crystalline core (PCL), whereas the other type lacks the core completely. It is noted that the curved structure of the adsorbed brushes can make it difficult to determine their exact length in some cases. The CPBs produced from backbones with the same DP had comparable lengths and length distributions. However, their appearance on mica (and probably also in solution) was quite different (Supporting Information S5). While [PCL$_{25}$-*b*-(PEGMA$_{98}$-*co*-GMA$_{16}$)]$_{2700}$ (Figure 2B) and [PEGMA$_{188}$-*co*-GMA$_{32}$]$_{2700}$ (Figure 2C) appeared to be quite similar on mica, the difference in appearance between [PCL$_{14}$-*b*-(PEGMA$_{94}$-*co*-GMA$_{16}$)]$_{7500}$ (Figure 2E) and [PEGMA$_{170}$-*co*-GMA$_{28}$]$_{7500}$ (Figure 2F) was more pronounced. The CPBs bearing a PCL core compartment appeared less coiled. The PCL core is expected to provide the respective brush with more rigidity and hence reduces the degree of coiling of the brush. DSC measurements further confirmed the PCL brush crystallizes between 24−28 °C (Supporting Information S6). In an aqueous environment, PCL is insoluble and this property should further contribute to the stiffness of the particles.[43−45] In addition, core−shell CPBs containing PCL as core material are able to form a crystalline core.[46,47] Figures 2B and 2E show the CPBs [PCL$_{25}$-*b*-(PEGMA$_{98}$-*co*-GMA$_{16}$)]$_{2700}$ and [PCL$_{14}$-*b*-(PEGMA$_{94}$-*co*-GMA$_{16}$)]$_{7500}$, respectively. Both CPBs appear relatively more rigid when compared to their counterparts without the PCL

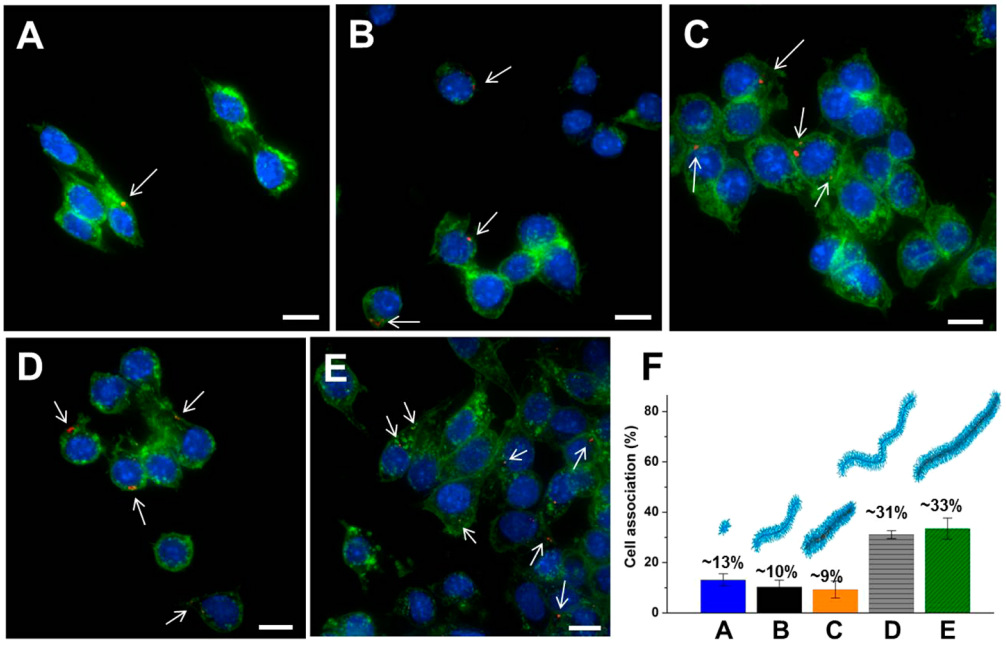

Figure 3. Deconvolution microscopy images of RAW 264.7 cells incubated (24 h) with 0.2 g·L^{-1} of AF647-labeled (A) [PEGMA$_{140}$-*co*-GMA$_{21}$]$_{112}$, (B) [PEGMA$_{188}$-*co*-GMA$_{32}$]$_{2700}$, (C) [PCL$_{25}$-*b*-(PEGMA$_{98}$-*co*-GMA$_{16}$)]$_{2700}$, (D) [PEGMA$_{170}$-*co*-GMA$_{28}$]$_{7500}$, and (E) [PCL$_{14}$-*b*-(PEGMA$_{94}$-*co*-GMA$_{16}$)]$_{7500}$, respectively. White arrows indicate internalized CPBs (red fluorescence). (F) Cell association of respective CPBs in A−E after 24 h incubation. The scale bars represent 10 μm.

core (Figures 2C and 2F). Particularly [PEGMA$_{170}$-*co*-GMA$_{28}$]$_{7500}$ shows a significantly more undulated structure compared to [PCL$_{14}$-*b*-(PEGMA$_{94}$-*co*-GMA$_{16}$)]$_{7500}$. The same phenomenon was observed for brushes deposited from aqueous solution (Supporting Information S7).

***In Vitro* Cell Association of CPBs.** To investigate the cell association of CPBs, we incubated AF647-labeled CPBs with *in vitro* cultured macrophages (RAW264.7) at different brush concentrations for 24 h. Flow cytometry was used to quantify cell association (Figure 3F). The overall cell association was rather low, considering the high polymer concentration (0.2 g·L^{-1}). While [PEGMA$_{140}$-*co*-GMA$_{21}$]$_{112}$ (Figure 3F, blue column) and [PEGMA$_{188}$-*co*-GMA$_{32}$]$_{2700}$ (Figure 3F, black column) showed almost the same amount of cellular interaction, the association of the longest CPBs [PEGMA$_{170}$-*co*-GMA$_{28}$]$_{7500}$ (Figure 3F, gray column) was almost three times higher (~30%). It is has been shown that particle shape and size may impact cell attachment and internalization.[4] Lowering the polymer brush concentration reduced the cell association even further (below 5%, see Supporting Information S8). Deconvolution microscopy confirmed the low cell association (Figure 3 and Supporting Information S9). Only a small number of cells internalized the CPBs (see white arrows in Figures 3A−E). Interestingly, the rigidified CPBs (containing a PCL core) showed very similar amounts of cell association when compared to their core-less analogues, indicating that the low-fouling nature of PEGMA might dominate the cellular interactions over altering the rigidity. In light of the low uptake of PEGMA-based CPBs by macrophages, and therefore the prospect of long-circulating behavior *in vivo*, we subsequently sought to investigate the *in vivo* performance of the CPBs in detail.

***In Vivo* Pharmacokinetics of CPBs.** To study the pharmacokinetics and biodistribution of CPBs and to evaluate the impact of the observed differences in length and rigidity on *in vivo* behavior, the CPBs were ^{3}H-labeled *via* CuAAC and intravenously administered to rats. The plasma concentration *versus* time profiles for CPBs (Figure 4) were established by scintillation counting of plasma samples taken at various time points following a 5 mg·kg^{-1} intravenous dose. Concentrations are expressed as μg equivalents of CPB per mL of plasma. Individual pharmacokinetic parameters were calculated using WinNonlin PK modeling software and summary parameters are shown in Table 2.

Increasing the Brush Aspect Ratio Increases Plasma Clearance of CPBs. In order to produce comparable samples, where only one parameter at a time was altered, CPB samples with different lengths were synthesized while the DP of the side chains was kept similar. Consequently, the diameter of the CPBs in solution was expected to be similar across all three samples. All examined CPBs showed prolonged plasma exposure. Thus, CPB plasma concentrations dropped by less than one log unit over a 24 h period and showed terminal half-lives >20 h. Across the series, increasing brush length resulted in small increases in Vd_{ss}, and larger increases in plasma clearance. Collectively this resulted in moderate decreases in terminal half-life with increases in brush length. Thus, the clearance of

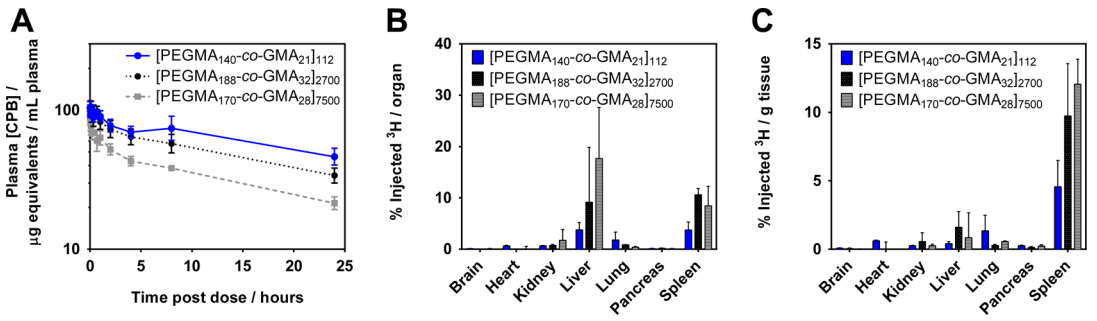

Figure 4. Pharmacokinetic and biodistribution data for CPBs of varying length after intravenous administration at 5 mg·kg^{-1} to rats: (A) Plasma concentration−time profiles. (B) Distribution of ^{3}H in organs after sacrifice at 24 h. (C) Percentage of ^{3}H in organs after sacrifice at 24 h, normalized for tissue mass. Values are mean ± SD (n = 3−4 rats).

TABLE 2. Overview of Calculated Pharmacokinetic Parameters

CPBs	$T_{1/2}$[a] (h)	Cl[a] (mL·h^{-1}·kg^{-1})	Vd_{ss}[a] (mL·kg^{-1})
[PEGMA$_{140}$-*co*-GMA$_{21}$]$_{112}$	29.3 ± 3.4	1.4 ± 0.2	59.2 ± 9.8
[PEGMA$_{188}$-*co*-GMA$_{32}$]$_{2700}$	21.2 ± 3.5	2.2 ± 0.3	64.6 ± 11.1
[PEGMA$_{170}$-*co*-GMA$_{28}$]$_{7500}$	20.4 ± 5.0	3.4 ± 0.5	92.6 ± 6.7
[PCL$_{25}$-*b*-(PEGMA$_{98}$-*co*-GMA$_{16}$)]$_{2700}$	26.4 ± 9.8	2.7 ± 0.7	92.9 ± 8.0
[PCL$_{14}$-*b*-(PEGMA$_{94}$-*co*-GMA$_{16}$)]$_{7500}$	18.9 ± 5.4	8.9 ± 1.3	225.0 ± 36.3

[a] $T_{1/2}$ = terminal half-life; Cl = clearance; Vd_{ss} = volume of distribution at steady state.

the shortest brush, [PEGMA$_{140}$-*co*-GMA$_{21}$]$_{112}$ (with a structure most closely resembling a sphere) was 1.4 ± 0.2 mL/h/kg, whereas for the longest brush, [PEGMA$_{170}$-*co*-GMA$_{28}$]$_{7500}$, with a measured length of 1150 ± 300 nm, clearance increased to 3.4 ± 0.5 mL/h/kg. Across the same constructs Vd_{ss} increased from 59.2 ± 9.8 to 92.6 ± 6.7 mL/kg. The trend in clearance was not proportional to the increase in brush length, and increases in brush length of ∼30-fold between [PEGMA$_{140}$-*co*-GMA$_{21}$]$_{112}$ and [PEGMA$_{170}$-*co*-GMA$_{28}$]$_{7500}$ resulted in only relatively small increases (2−3 fold) in CPB clearance. Interestingly, this finding is the opposite of the length-dependent behavior previously reported for self-assembled filomicelle materials.[37] That study showed an increase in systemic circulation time with increasing length. 2 μm filomicelles were reported to have a circulation half-life of approximately 2 days, whereas the 18 μm analogues showed more than double that (approximately 4.5 days). However, the conclusion drawn for the filomicelle materials, which are not necessarily stable to shear forces due to their self-assembled nature, was that the filomicelles broke down over time and smaller fragments were phagocytosed, while the remainder persisted in circulation. The result of this was that although some residual fragments of the longest (18 μm) filomicelles could still be detected up to 7 days post dosing, this was not due to the longer filomicelles completely evading recognition. We attribute the observation of the opposite trend here for the CPBs to the stability of the CPB backbone when compared with the self-assembled cylindrical micelles. Thus, the backbone stability of the CPBs makes the model of steady attrition of the highest aspect ratio materials unlikely to apply. In turn, this leads to the outcome of increasing size giving rise to increased splenic filtration and phagocytic clearance by the cells of the MPS. This difference in behavior is supported by the finding that filomicelles with a cross-linked core were cleared within hours as opposed to days.[37] Although no length-dependent behavior was described for the cross-linked materials,[37] the finding suggests that cross-linked cylindrical objects behave differently to those that are self-assembled and not further stabilized postassembly.

Increasing Brush Aspect Ratio Results in Increased Deposition in MPS Organs. The *in vivo* biodistribution of the CPBs in major organs (brain, heart, kidney, liver, lung, pancreas, and spleen) was determined by analyzing ^{3}H in tissues harvested 24 h post dosing at 5 mg·kg^{-1}. The percentage of injected ^{3}H recovered in tissues is given in Figure 4B. As expected, the most significant uptake was evident in the spleen and liver, supporting a mechanism of MPS recognition and clearance.[48,49] Panel C gives the organ uptake normalized per gram of organ tissue and demonstrates the relative efficiency of splenic filtration in the clearance of CPBs of all lengths. This is not unexpected since the molecular weight and polymeric architecture of the, albeit unimolecular, CPBs is sufficient to push them to behave in a manner that is particle-like. The systemic clearance of polymers is thought to proceed by two different mechanisms, depending on molecular weight. Below ∼48 kDa the renal clearance of small molecules leads to reduced exposure.[50] At sizes above the renal clearance limit and where phagocytosis is inhibited by PEGylation, long circulation behavior is commonly evident. However, as the size approaches ∼150−200 nm, particle-like behavior leads to increased MPS recognition and filtration by the spleen.[51] Studies of particles of varying size have generally shown that increased particle size correlates to increased clearance rates, although this finding is better understood for spherical systems.[52] Examples of anisotropic materials are more limited. In terms of *in vivo* behavior, CPBs appear to exhibit what could

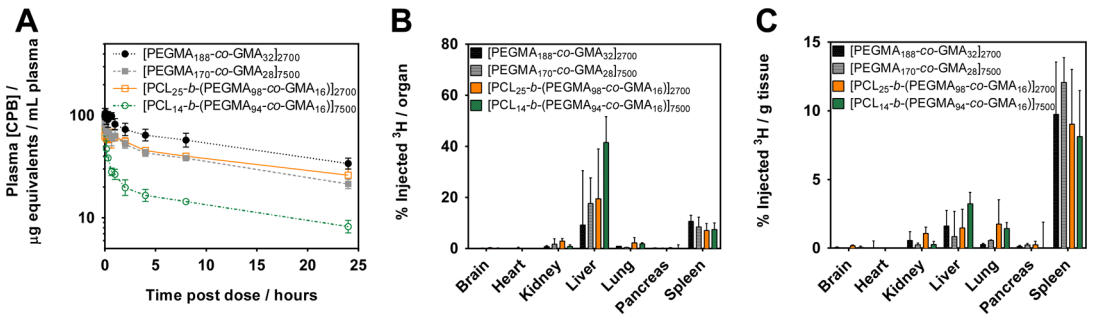

Figure 5. Pharmacokinetic and biodistribution data for ^{3}H-labeled CPB analogues in the presence and absence of a PCL core after intravenous administration at 5 mg·kg^{-1} to rats: (A) Plasma concentration−time profiles. (B) Distribution of ^{3}H in organs after sacrifice at 24 h. (C) Percentage of ^{3}H in organs after sacrifice at 24 h, normalized for tissue mass. Values are mean ± SD (n = 3−4 rats).

be described as classic particle-like behavior, despite being themselves unimolecular entities. This is in contrast to what has been shown recently for hydrophilic carbon nanotubes, which were excreted into urine within 4 h, despite being relatively rigid and having lengths on a micrometer scale.[50] These contrasting data suggest that the mechanisms of clearance of anisotropic materials are likely to be highly material dependent, among other factors.

Increasing CPB Rigidity Decreases Plasma Residence Time. Figure 5A contrasts the plasma concentration−time profiles for [PEGMA$_{188}$-*co*-GMA$_{32}$]$_{2700}$ and [PEGMA$_{170}$-*co*-GMA$_{28}$]$_{7500}$ with profiles for CPBs based on the same backbone, but with an added PCL core compartment, [PCL$_{25}$-*b*-(PEGMA$_{98}$-*co*-GMA$_{16}$)]$_{2700}$ and [PCL$_{14}$-*b*-(PEGMA$_{94}$-*co*-GMA$_{16}$)]$_{7500}$. The PCL core is not soluble in water and leads to more cylindrical and less random coiled structures with increased rigidity (Figure 2, Figure S6). The rigidified brushes showed differences in both clearance and volume of distribution, and these trends were most apparent for the largest construct ([PCL$_{14}$-*b*-(PEGMA$_{94}$-*co*-GMA$_{16}$)]$_{7500}$). Thus, when compared to the CPBs without the PCL core, the rigidified analogues demonstrated more rapid clearance from plasma. This effect was more marked for the longest CPBs for which the calculated clearance values were 8.9 ± 1.3 mL·h^{-1}·kg^{-1} for [CL$_{14}$-*b*-(PEGMA$_{94}$-*co*-GMA$_{16}$)]$_{7500}$ compared with 3.4 ± 0.5 mL·h^{-1}·kg^{-1} for [PEGMA$_{170}$-*co*-GMA$_{28}$]$_{7500}$. In the case of the midlength brushes the difference was less pronounced, with clearance being 2.7 ± 0.7 mL·h^{-1}·kg^{-1} for [PCL$_{25}$-*b*-(PEGMA$_{98}$-*co*-GMA$_{16}$)]$_{2700}$ compared with 2.2 ± 0.3 mL·h^{-1}·kg^{-1} for [PEGMA$_{188}$-*co*-GMA$_{32}$]$_{2700}$. Interestingly, the most striking difference for the larger, more rigid system was an increase in volume of distribution from 92.6 ± 6.7 mL·kg^{-1} for [PEGMA$_{170}$-*co*-GMA$_{28}$]$_{7500}$ to 225 ± 36.3 mL·kg^{-1} for [PCL$_{14}$-*b*-(PEGMA$_{94}$-*co*-GMA$_{16}$)]$_{7500}$, evidenced by the rapid initial drop in plasma concentration over the first 1−2 h. The biodistribution data for the rigidified CPBs with PCL cores (Figures 5B and 5C) suggest that the differences in volume of distribution and clearance may increase the amount of ^{3}H in the liver after 24 h, particularly for the longer CPBs. In contrast, there was no evidence for increased uptake in the spleen.

The high uniformity and stability of the CPBs may offer advantages in more predictable behavior *in vivo* compared with self-assembled materials. The high degree of control that is possible in terms of architecture and functionalization is attractive in an area where control over cargo loading, release, and organ deposition profile is critical. The *in vivo* data reported herein provide a first step toward the realization of this potential, and show that relatively large CPBs can be constructed with long circulation half-lives, which is consistent with the potential for accumulation in tumors *via* the enhanced permeability and retention (EPR) effect.[53] Previous studies have shown that CPBs may be drug loaded with high efficiency.[31,32]

CONCLUSIONS

The modular synthetic assembly of CPBs from low-fouling materials such as PEG, including labeling with radiolabel tracers *via* click chemistry, allowed the fabrication and evaluation of discrete functional nanostructures of various aspect ratios and altered rigidity. Fine control over particle properties enabled an initial investigation of the impact of size, aspect ratio and rigidity on *in vivo* pharmacokinetic behavior in a rat model. The CPBs exhibited long circulation half-lives, in some cases exceeding 24 h, despite their high molecular weights (ranging from millions to hundreds of millions g·mol^{-1}). Interestingly, changes in brush composition and rigidity had limited effect on their behavior in *in vitro* cell culture experiments. However, the incorporation of a crystalline core compartment into the CPBs resulted in more rapid clearance *in vivo*, suggesting that the flexibility of anisotropic materials plays a significant role in their filtration and clearance. The ability to engineer CPB composition, nanostructural shape and particle behavior has the potential to provide alternative materials to address challenges in *in vivo* drug delivery and also imaging applications, where the possibility to tailor distribution patterns is

particularly attractive. Investigations into control over drug loading and release in CPBs, and the impact of changes to aspect ratio on accumulation in xenograft models, are part of our ongoing research.

EXPERIMENTAL SECTION

Materials. High purity (Milli-Q) water with a resistivity of >18.2 MΩ·cm was obtained from an inline Millipore RiOs/Origin water purification system. Deuterium oxide (D_2O), copper(I) bromide (CuBr, 98%), α-bromoisobutyryl bromide (98%), propargylamine (98%), glycidyl methacrylate (GMA, 97%), ε-caprolactone (CL, 97%), tin(II) 2-ethylhexanoate (95%), 2-(trimethylsilyloxy)ethyl methacrylate (TMS-HEMA, 96%), poly(ethylene glycol) methyl ether methacrylate (PEGMA, average M_n = 300 g·mol^{-1}), and *N*,*N*,*N*′,*N*″,*N*″-pentamethyl-diethylenetriamine (PMDETA, 99%), triethylamine (TEA, 99.5%), and anhydrous pyridine and tetrahydrofuran (THF) were obtained from Sigma-Aldrich. Alexa Fluor 647 cadaverine (AF647) was purchased from Invitrogen (Australia). 4-Azidosalicylic acid (ring-5-^{3}H) was purchased from American Radiolabeled Chemicals, Inc. (Saint Louis, MO, USA). Ultima Gold scintillation cocktail and Soluene-350 tissue solubilizer were obtained from (PerkinElmer, Inc., Waltham, MA, USA). Saline for injection was purchased in 100 mL polyethylene bags from Baxter Healthcare Pty., Ltd. (Old Toongabbie, NSW, Australia). DBL Heparin Sodium Injection BP was purchased from Hospira (Australia). Phosphate buffered saline (PBS) was received as tablets from Sigma-Aldrich (NSW, Australia) and made up at a concentration of two tablets in 400 mL of Milli-Q water. All chemicals were used as received, except GMA, CL and tin(II) 2-ethylhexanoate, which were freshly distilled prior to use. All methacrylic monomers were passed through a short silica gel column prior to polymerization to remove the inhibitor.

Characterization Methods. Nuclear magnetic resonance (^{1}H NMR) spectra were recorded in deuterated solvents using a 400 MHz Varian INOVA system at 25 °C. Noncontact mode atomic force microscopy (AFM) imaging was performed in air using a Cypher S (Asylum Research) with tapping-mode cantilevers (4 N·m^{-1}, Tap150-G, Budget Sensors, Bulgaria). Images were post-treated using IGOR Pro image processing software. Prior to AFM measurement, freshly cleaved mica was dipped into a solution of CPBs (~0.2 g·L^{-1}) and allowed to dry under a stream of nitrogen. DSC measurements were performed in N_2 using a PerkinElmer Sapphire DSC with a temperature scan rate of 10 K·min^{-1}. Flow cytometry analysis was performed on an Apogee A50-Micro Flow System. At least 1 × 10^5 cells were counted and experiments were performed in triplicates. Cellular interactions were studied using a DeltaVision (Applied Precision, USA) microscope with a 60× 1.52 NA oil objective for deconvolution fluorescence microscopy with a standard FITC/TRITC/CY5 filter set. Images were processed with Imaris (Bitplane) using the maximum intensity projection.

Preparation of the Cylindrical Polymer Brushes (CPBs). The CPBs were synthesized through the combination of various polymerization techniques, such as anionic, ring opening and atom transfer radical polymerization. The stepwise build-up from a polyinitiator backbone to a CPB is explained in detail below. Table S1 in the Supporting Information (S10) gives an overview of the synthesized CPBs used in this study.

Synthesis of Polymer Backbones. The PHEMA backbones were obtained through deprotection of various poly(2-(trimethylsiloxy)ethyl methacrylate) (PTMS-HEMA). The PTMS-HEMA backbones were either synthesized *via* anionic polymerization, as previously reported by Mori and co-workers[54] or *via* ATRP according to a procedure of Matyjaszewski and co-workers.[55] The deprotection to PHEMA was performed in methanol using acetic acid (90/10 v/v). In the following, PHEMA was either used directly as a polyinitiator for the ROP of CL or modified to an ATRP polyinitiator. To introduce ATRP initiators, PHEMA was reacted with a 1.5-fold molar excess of 2-bromoisobutyryl bromide in either anhydrous pyridine (for backbones with DP = 2700 and 7500) or in anhydrous THF (for the short backbone) containing a 2-fold molar excess of triethylamine (TEA).

Synthesis of Cylindrical Polymer Brushes [PEGMA$_x$-*co*-GMA$_y$]$_z$. Ten mg (36 μM) PBIEM$_z$ (z = 112, 2700, or 7500), PMDETA and a monomer mixture of PEGMA and GMA were mixed with 17 g of anisole in a Schlenk flask. Subsequently, the mixture was degassed with three freeze−pump−thaw cycles before CuBr was introduced. The polymerization was performed at 60 °C. The ratios of [PBIEM]:[PEGMA]:[GMA]:[PMDETA]:[CuBr] were 1:425:75:1:1. The polymerization was monitored *via* ^{1}H NMR and quenched at the desired conversion by cooling and exposing it to air. The polymer solution was passed through a short silica gel column before it was precipitated into cold hexanes. The precipitate was immediately dissolved as well as dialyzed in acetone. To calculate the brush composition we used previously reported grafting efficiencies from PBIEM of 50% for PEGMA.[56]

Synthesis of Cylindrical Polymer Brushes [PCL$_v$]$_z$. [PCL$_v$]$_z$ (z = 2700 or 7500) CPBs were synthesized as previously reported.[43,44] Briefly, PHEMA was dissolved in dry caprolactone and water traces were distilled off in the presence of benzene. Afterward, the mixture was degassed by three freeze−pump−thaw cycles. The ring-opening polymerization (ROP) of CL was catalyzed by the addition of tin(II) 2-ethylhexanoate at 125 °C. The polymerization was allowed to proceed until the mixture became highly viscous. The polymerization was quenched by cooling and exposing to air and then diluted with THF and precipitated into cold cyclohexane. The PCL homopolymer brushes were precipitated twice into a cold water/methanol mixture (10/90 v/v) and then freeze-dried from dioxane. [PCL$_v$]$_z$ was then reacted with a 1.5-fold molar excess of 2-bromoisobutyryl bromide and a 2-fold molar excess of triethylamine (TEA) in dry THF to functionalize the PCL brush with ATRP initiating groups. After 24 h of stirring at room temperature, the functionalized polymer was concentrated by solvent evaporation, precipitated in a cold water/methanol mixture (80/20 v/v) and freeze-dried from dioxane.

Synthesis of the Cylindrical Core−Shell Polymer Brush [PCL$_v$-(PEGMA$_x$-*co*-GMA$_y$)]$_z$. 3.4 μM [PCL$_{25}$]$_{2700}$ or [PCL$_{14}$]$_{7500}$ were dissolved in 6 mL of anisole and mixed with PMDETA and a monomer mixture of PEGMA and GMA in a Schlenk flask. The mixture was then degassed with three freeze−pump−thaw cycles before CuBr was introduced. The ratios of [PCL]:[PEGMA]:[GMA]:[PMDETA]:[CuBr] were 1:850:150:1:1. The polymerization was performed at 70 °C. The polymerization was monitored *via* ^{1}H NMR and quenched at the desired conversion by cooling and exposing it to air. The polymer solution was passed through a short silica gel column before it was precipitated into cold hexanes. The precipitate was immediately dissolved in acetone and dialyzed into THF. To calculate the brush composition we used previously reported grafting efficiencies of PCL brushes of 90%.[43]

Synthesis of AF647-Labeled CPBs. Thirty mg of the CPBs containing GMA was dissolved in 5 mL of dry DMSO. Subsequently, 10 μL of AF647 cadaverine and 50 μL of TEA were added. After another 10 min of argon bubbling, the reaction mixture was allowed to stir overnight at 55 °C. In order to purify the modified CPBs, the reaction mixture was first dialyzed into acetone, and then further dialyzed into Milli-Q water.

Synthesis of Alkyne-Modified CPBs. Thirty mg of the CPBs containing GMA was dissolved in 5 mL dry DMSO and deoxygenated for 15 min by bubbling argon. Subsequently, 10 μL of propargylamine and 100 μL of TEA were added. After another 10 min of argon bubbling, the reaction mixture was allowed to stir overnight at 50 °C. In order to purify the modified CPBs, the reaction mixture was first dialyzed into acetone, and then further dialyzed into ethanol.

Radiolabeling of CPBs. 4-Azidosalicylic acid [ring-5-^{3}H] (10 μL as purchased, nominally 10 μCi based on the quoted concentration of stock [1 Ci·L^{-1} in ethanol]) was added with stirring to

CPBs suspended in polar solvent (Milli-Q water or ethanol) (3 mL). Suspension concentrations were in the range 4.4−10.0 $g \cdot L^{-1}$. Copper sulfate (700 μg) and sodium ascorbate (1 mg), both as solutions in Milli-Q water, were added and stirring was continued overnight. Unreacted 4-azidosalicylic acid and copper catalyst were removed from the reaction mixture by dialysis against ethanol followed by Milli-Q water, or Milli-Q water alone over a number of days. At this stage an aliquot of each sample (200 μL) was removed from the dialysis tubing and allowed to evaporate to dryness in a microcentrifuge tube of known mass. The tube was reweighed to establish the sample concentration. Samples were diluted to a standard concentration of 1.5 $g \cdot L^{-1}$ with PBS. This concentration was based on a standard administered dose of 5 $mg \cdot kg^{-1}$ in 1 mL, to a rat with an average weight of 300 g. CPB suspensions were stored at 4 °C until used.

Determination of Noncovalently Bound Label. A sample of radiolabeled CPBs (volume and concentration dependent on particular sample identification) was diluted into Milli-Q water to give a sample of known dilution and volume in the range 500−1000 μL. An aliquot of the diluted suspension (150 μL) was added to a Nanosep centrifugal device with a molecular weight cut off (MWCO) of 300 kDa (Pall Corporation, Port Washington, NY, USA). The sample was centrifuged at 5000*g* for 5 min. An aliquot of the resulting filtrate (50 μL) was added to an Ultima Gold scintillation cocktail (2 mL) and homogenized by vortex mixing. A sample of diluted radiolabeled CPB suspension before filtration (50 μL), and a sample of CPB suspension before ^{3}H modification (50 μL, concentration matched to that of labeled dilution) were also suspended in Ultima Gold (2 mL) and thoroughly mixed. All samples were measured using a PerkinElmer Tri-Carb 2800TR Liquid Scintillation Analyzer (PerkinElmer, Inc., Waltham, Massachusetts, USA). On the basis of the high MW of CPBs, it is assumed that the measured activity of the filtrate arises from 4-azidosalicylic acid ^{3}H molecules that are not covalently bound to CPBs.

Activity Determination. The specific activity of CPBs after dilution was determined by adding aliquots of a radiolabeled CPB suspension (10 μL) to an Ultima Gold scintillation cocktail (2 mL) in triplicate. Samples were well homogenized using a vortex mixer and measured by scintillation counting. The mean of the triplicate values was used for subsequent calculations.

Cell Culture, Cell Fixation and Staining. RAW264.7 cells were cultured in regular growth medium consisting of high glucose DMEM supplemented with 10% fetal bovine serum (FBS) and 1% Glutamax at 37 °C, in a 5% CO_2 humidified incubator. The cells were routinely passaged until 80−90% confluence. Cells were trypsinized and plated into 24-well plates (5×10^4 cells per well). The cells were allowed to adhere overnight. Subsequently, the cells were incubated with CPBs for up to 24 h. After incubation, the cells were gently washed twice with warm DPBS before being trypsinized and studied by flow cytometry. For imaging, RAW264.7 cells were plated at 2.5×10^4 cells per well into 8-well Lab-Tek I chambered coverglass slides (Thermo Fisher Scientific, Rochester) and allowed to adhere overnight. Cells were then incubated with CPBs at a concentration of 0.2 or 0.05 $g \cdot L^{-1}$ for 24 h (37 °C, 5% CO_2). Subsequently, cells were gently washed with warm PBS three times and fixed using 4% paraformaldehyde (PFA) for 10 min at room temperature. The cell membrane was stained with Alexa Fluor 488 wheat germ agglutinin (WGA) (3 μL, 2.5 $mg \cdot mL^{-1}$) incubated at room temperature for 15 min. The cell nucleus was stained at room temperature (10 min) using Hoechst Fluorescent Stain. Images were taken in PBS solution.

Animal Details. *In vivo* studies were carried out using male Sprague−Dawley rats (250−350 g) based on procedures previously described.[57] All animal studies were approved by the Monash Institute of Pharmaceutical Sciences Animal Ethics Committee, Monash University, Parkville, VIC, Australia.

Intravenous Pharmacokinetic (PK) Studies. Prior to CPB administration, rats were anaesthetized under isoflurane and the jugular vein and carotid artery surgically cannulated with polyethylene tubing (0.96 × 0.58 mm, Paton Scientific, Victor Harbour, Australia) to facilitate intravenous administration and blood collection, respectively.[58] Cannulas were flushed with heparinized saline (2 $IU \cdot mL^{-1}$) to maintain patency. Rats were housed in metabolic cages and allowed to recover overnight prior to dosing, with water provided *ad libitum* throughout the experiment. Animals were fasted up to 10 h prior to and 8 h after dose administration. Solutions of CPBs in PBS were prepared so as to give a dose equivalent to 5 mg per kg per 1 mL infusion. Prepared solutions were dosed intravenously as an infusion (1 $mL \cdot min^{-1}$) *via* the jugular cannula over a period of 1 min (n = 4 per formulation). Following infusion the cannula was flushed with 250 μL of heparinized saline to clear the dead volume. Blood samples (200 μL) were obtained from the carotid artery cannula prior to infusion (predose), immediately after infusion (t = 0), and at 2, 5, 10, 20, 40, 60, 120, 240, 480, and 1440 min. Blood samples were centrifuged at 1000*g* for 5 min to separate plasma. Plasma samples (50 μL) were added to an Ultima Gold scintillation cocktail (2 mL) for scintillation measurement. Noncompartmental pharmacokinetic parameters (clearance, volume of distribution) were calculated using Phoenix 64 Software (WinNonlin version 6.3, Pharsight Corporation, CA, USA).

Biodistribution Studies. At the conclusion of blood sampling (1440 min [24 h]) rats were sacrificed by administration of a lethal dose of sodium pentobarbital into the jugular vein cannula. Brain, heart, kidney, liver, lungs, pancreas and spleen tissues were removed by dissection, weighed and frozen (−20 °C) until processed. Whole organs were placed in gentleMACS C tubes (Miltenyi Biotech Australia Pty., Ltd., NSW, Australia) and partially disrupted using scissors. Milli-Q water (5 mL for liver samples, 10 mL for all other tissues) was added before samples were homogenized using a gentleMACS dissociator (Miltenyi Biotech Australia Pty., Ltd., NSW, Australia) running a standard C tubes program. Two samples of each homogenate were aliquoted by volume into 20 mL polypropylene scintillation vials, based on the wt % of organ contained. The target tissue sample masses were 40, 70, and 100 mg for liver, kidney, and all other organs, respectively. A 1:1 mixture of Soluene-350:isopropyl alcohol (IPA) (4 mL) was added to each sample. Samples were kept at 60 °C overnight to allow tissues to digest. Samples were cooled to room temperature and hydrogen peroxide (30% w/v, 200 μL) was added in 2 × 100 μL aliquots. After bubbling had ceased (approximately 30 min) Ultima Gold (10 mL) was added and samples were thoroughly homogenized using a vortex mixer and stored at 4 °C, in dark conditions without agitation for at least 96 h. Sample scintillation was then measured for one sample of each tissue homogenate with the counter temperature maintained at 12 °C. This measurement established the approximate level of activity in each sample. Subsequently one sample from each pair was spiked with a suitable solution of 4-azidosalicylic acid (ring-5-^{3}H) of known activity based on the approximate activity measured in order to determine the efficiency of extraction of the radiolabel from tissue samples. After thorough mixing, all samples were allowed to rest for a further 96 h at 4 °C. Before sample measurement the scintillation counter was cooled to 12 °C. Samples were loaded in batches of 12 to prevent significant temperature changes during the course of the measurements. Tissue samples from untreated rats were also processed using the same method to provide a background count for equivalent masses of each tissue type.

The acquired raw data was used to establish an efficiency value for each sample using the following equation:

$$\text{efficiency} = \frac{\text{spiked tissue}_{\text{dpm}} - \text{tissue}_{\text{dpm, uncorr}}}{\text{spiked solution}_{\text{dpm}}} \quad (1)$$

where spiked $\text{tissue}_{\text{dpm}}$ is the radioactivity measured in the spiked sample, $\text{tissue}_{\text{dpm,uncorr}}$ is the radioactivity in the unspiked sample, and $\text{spike solution}_{\text{dpm}}$ is the known amount of radioactivity added to the spiked sample. The calculated efficiency value was used to correct the dpm value for each measured sample to eliminate the effect of quenching, which may have resulted from sample processing. This was performed using the following relationship:

$$\text{tissue}_{\text{dpm, corr}} = \frac{\text{tissue}_{\text{dpm, uncorr}}}{\text{efficiency}} \quad (2)$$

where $tissue_{dpm,corr}$ is taken to give the true sample activity. The activity of the whole organ was calculated based on the fraction of total organ mass contained within the measured sample.

Conflict of Interest: The authors declare no competing financial interest.

Acknowledgment. This research was conducted and funded by the Australian Research Council Centre of Excellence in Convergent Bio-Nano Science and Technology (project number CE140100036). This work was also supported by the Australian Research Council under the Australian Laureate Fellowship (F.C., FL120100030) scheme. M.M. acknowledges The University of Melbourne for a McKenzie Fellowship.

Supporting Information Available: Synthetic procedure for the stepwise buildup of CPBs, including an overview of polymer backbones and CPBs used in this study. Additional characterization, including *in vitro* cell studies, DLS, AFM, DSC, scintillation counts and IR measurements. This material is available free of charge *via* the Internet at http://pubs.acs.org.

REFERENCES AND NOTES

1. Torchilin, V. P. Micellar Nanocarriers: Pharmaceutical Perspectives. *Pharm. Res.* **2007**, *24*, 1–16.
2. Chithrani, B. D.; Chan, W. C. W. Elucidating the Mechanism of Cellular Uptake and Removal of Protein-Coated Gold Nanoparticles of Different Sizes and Shapes. *Nano Lett.* **2007**, *7*, 1542–1550.
3. Markovsky, E.; Baabur-Cohen, H.; Eldar-Boock, A.; Omer, L.; Tiram, G.; Ferber, S.; Ofek, P.; Polyak, D.; Scomparin, A.; Satchi-Fainaro, R. Administration, Distribution, Metabolism and Elimination of Polymer Therapeutics. *J. Controlled Release* **2012**, *161*, 446–460.
4. Sharma, G.; Valenta, D. T.; Altman, Y.; Harvey, S.; Xie, H.; Mitragotri, S.; Smith, J. W. Polymer Particle Shape Independently Influences Binding and Internalization by Macrophages. *J. Controlled Release* **2010**, *147*, 408–412.
5. Florez, L.; Herrmann, C.; Cramer, J. M.; Hauser, C. P.; Koynov, K.; Landfester, K.; Crespy, D.; Mailänder, V. How Shape Influences Uptake: Interactions of Anisotropic Polymer Nanoparticles and Human Mesenchymal Stem Cells. *Small* **2012**, *8*, 2222–2230.
6. Yue, J.; Liu, S.; Xie, Z.; Xing, Y.; Jing, X. Size-Dependent Biodistribution and Antitumor Efficacy of Polymer Micelle Drug Delivery Systems. *J. Mater. Chem. B* **2013**, *1*, 4273–4280.
7. Owens Iii, D. E.; Peppas, N. A. Opsonization, Biodistribution, and Pharmacokinetics of Polymeric Nanoparticles. *Int. J. Pharm.* **2006**, *307*, 93–102.
8. Grayson, S. M.; Godbey, W. T. The Role of Macromolecular Architecture in Passively Targeted Polymeric Carriers for Drug and Gene Delivery. *J. Drug Targeting* **2008**, *16*, 329–356.
9. Balogh, L.; Nigavekar, S. S.; Nair, B. M.; Lesniak, W.; Zhang, C.; Sung, L. Y.; Kariapper, M. S. T.; El-Jawahri, A.; Llanes, M.; Bolton, B.; *et al.* Significant Effect of Size on the *in Vivo* Biodistribution of Gold Composite Nanodevices in Mouse Tumor Models. *Nanomed.: Nanotechnol., Biol. Med.* **2007**, *3*, 281–296.
10. Nasongkla, N.; Chen, B.; Macaraeg, N.; Fox, M. E.; Fréchet, J. M. J.; Szoka, F. C. Dependence of Pharmacokinetics and Biodistribution on Polymer Architecture: Effect of Cyclic *versus* Linear Polymers. *J. Am. Chem. Soc.* **2009**, *131*, 3842–3843.
11. Imran ul-haq, M.; Lai, B. F. L.; Chapanian, R.; Kizhakkedathu, J. N. Influence of Architecture of High Molecular Weight Linear and Branched Polyglycerols on Their Biocompatibility and Biodistribution. *Biomaterials* **2012**, *33*, 9135–9147.
12. Fox, M. E.; Szoka, F. C.; Fréchet, J. M. J. Soluble Polymer Carriers for the Treatment of Cancer: The Importance of Molecular Architecture. *Acc. Chem. Res.* **2009**, *42*, 1141–1151.
13. Maldiney, T.; Richard, C.; Seguin, J.; Wattier, N.; Bessodes, M.; Scherman, D. Effect of Core Diameter, Surface Coating, and PEG Chain Length on the Biodistribution of Persistent Luminescence Nanoparticles in Mice. *ACS Nano* **2011**, *5*, 854–862.
14. Decuzzi, P.; Godin, B.; Tanaka, T.; Lee, S. Y.; Chiappini, C.; Liu, X.; Ferrari, M. Size and Shape Effects in the Biodistribution of Intravascularly Injected Particles. *J. Controlled Release* **2010**, *141*, 320–327.
15. Champion, J. A.; Mitragotri, S. Role of Target Geometry in Phagocytosis. *Proc. Natl. Acad. Sci. U. S. A.* **2006**, *103*, 4930–4934.
16. Venkataraman, S.; Hedrick, J. L.; Ong, Z. Y.; Yang, C.; Ee, P. L. R.; Hammond, P. T.; Yang, Y. Y. The Effects of Polymeric Nanostructure Shape on Drug Delivery. *Adv. Drug Delivery Rev.* **2011**, *63*, 1228–1246.
17. Champion, J. A.; Katare, Y. K.; Mitragotri, S. Particle Shape: A New Design Parameter for Micro- and Nanoscale Drug Delivery Carriers. *J. Controlled Release* **2007**, *121*, 3–9.
18. Wu, M.; Shi, J.; Fan, D.; Zhou, Q.; Wang, F.; Niu, Z.; Huang, Y. Biobehavior in Normal and Tumor-Bearing Mice of Tobacco Mosaic Virus. *Biomacromolecules* **2013**, *14*, 4032–4037.
19. Bruckman, M. A.; Randolph, L. N.; VanMeter, A.; Hern, S.; Shoffstall, A. J.; Taurog, R. E.; Steinmetz, N. F. Biodistribution, Pharmacokinetics, and Blood Compatibility of Native and Pegylated Tobacco Mosaic Virus Nano-Rods and -Spheres in Mice. *Virology* **2014**, *449*, 163–173.
20. Huang, X.; Peng, X.; Wang, Y.; Wang, Y.; Shin, D. M.; El-Sayed, M. A.; Nie, S. A Reexamination of Active and Passive Tumor Targeting by Using Rod-Shaped Gold Nanocrystals and Covalently Conjugated Peptide Ligands. *ACS Nano* **2010**, *4*, 5887–5896.
21. Huang, X.; Li, L.; Liu, T.; Hao, N.; Liu, H.; Chen, D.; Tang, F. The Shape Effect of Mesoporous Silica Nanoparticles on Biodistribution, Clearance, and Biocompatibility *in Vivo*. *ACS Nano* **2011**, *5*, 5390–5399.
22. Cherukuri, P.; Gannon, C. J.; Leeuw, T. K.; Schmidt, H. K.; Smalley, R. E.; Curley, S. A.; Weisman, R. B. Mammalian Pharmacokinetics of Carbon Nanotubes Using Intrinsic near-Infrared Fluorescence. *Proc. Natl. Acad. Sci. U. S. A.* **2006**, *103*, 18882–18886.
23. Wang, H.; Wang, J.; Deng, X.; Sun, H.; Shi, Z.; Gu, Z.; Liu, Y.; Zhaoc, Y. Biodistribution of Carbon Single-Wall Carbon Nanotubes in Mice. *J. Nanosci. Nanotechnol.* **2004**, *4*, 1019–1024.
24. Liu, Z.; Cai, W.; He, L.; Nakayama, N.; Chen, K.; Sun, X.; Chen, X.; Dai, H. *In Vivo* Biodistribution and Highly Efficient Tumour Targeting of Carbon Nanotubes in Mice. *Nat. Nanotechnol.* **2007**, *2*, 47–52.
25. Merkel, T. J.; Jones, S. W.; Herlihy, K. P.; Kersey, F. R.; Shields, A. R.; Napier, M.; Luft, J. C.; Wu, H.; Zamboni, W. C.; Wang, A. Z.; *et al.* Using Mechanobiological Mimicry of Red Blood Cells to Extend Circulation Times of Hydrogel Microparticles. *Proc. Natl. Acad. Sci. U. S. A.* **2011**, *108*, 586–591.
26. Perry, J. L.; Reuter, K. G.; Kai, M. P.; Herlihy, K. P.; Jones, S. W.; Luft, J. C.; Napier, M.; Bear, J. E.; DeSimone, J. M. PEGylated Print Nanoparticles: The Impact of Peg Density on Protein Binding, Macrophage Association, Biodistribution, and Pharmacokinetics. *Nano Lett.* **2012**, *12*, 5304–5310.
27. Zhang, M.; Müller, A. H. E. Cylindrical Polymer Brushes. *J. Polym. Sci., Part A: Polym. Chem.* **2005**, *43*, 3461–3481.
28. Sheiko, S. S.; Sumerlin, B. S.; Matyjaszewski, K. Cylindrical Molecular Brushes: Synthesis, Characterization, and Properties. *Prog. Polym. Sci.* **2008**, *33*, 759–785.
29. Huang, K.; Jacobs, A.; Rzayev, J. *De Novo* Synthesis and Cellular Uptake of Organic Nanocapsules with Tunable Surface Chemistry. *Biomacromolecules* **2011**, *12*, 2327–2334.
30. Zhao, P.; Liu, L.; Feng, X.; Wang, C.; Shuai, X.; Chen, Y. Molecular Nanoworm with PCL Core and PEO Shell as a Non-Spherical Carrier for Drug Delivery. *Macromol. Rapid Commun.* **2012**, *33*, 1351–1355.
31. Johnson, J. A.; Lu, Y. Y.; Burts, A. O.; Lim, Y.-H.; Finn, M. G.; Koberstein, J. T.; Turro, N. J.; Tirrell, D. A.; Grubbs, R. H. Core-Clickable PEG-Branch-Azide Bivalent-Bottle-Brush

Polymers by ROMP: Grafting-through and Clicking-To. *J. Am. Chem. Soc.* **2010**, *133*, 559–566.
32. Johnson, J. A.; Lu, Y. Y.; Burts, A. O.; Xia, Y.; Durrell, A. C.; Tirrell, D. A.; Grubbs, R. H. Drug-Loaded, Bivalent-Bottle-Brush Polymers by Graft-through ROMP. *Macromolecules* **2010**, *43*, 10326–10335.
33. Chen, Y. Shaped Hairy Polymer Nanoobjects. *Macromolecules* **2012**, *45*, 2619–2631.
34. Liao, L.; Liu, J.; Dreaden, E. C.; Morton, S. W.; Shopsowitz, K. E.; Hammond, P. T.; Johnson, J. A. A Convergent Synthetic Platform for Single-Nanoparticle Combination Cancer Therapy: Ratiometric Loading and Controlled Release of Cisplatin, Doxorubicin, and Camptothecin. *J. Am. Chem. Soc.* **2014**, *136*, 5896–5899.
35. Rzayev, J. Molecular Bottlebrushes: New Opportunities in Nanomaterials Fabrication. *ACS Macro Lett.* **2012**, *1*, 1146–1149.
36. Christian, D. A.; Cai, S.; Garbuzenko, O. B.; Harada, T.; Zajac, A. L.; Minko, T.; Discher, D. E. Flexible Filaments for *in Vivo* Imaging and Delivery: Persistent Circulation of Filomicelles Opens the Dosage Window for Sustained Tumor Shrinkage. *Mol. Pharmaceutics* **2009**, *6*, 1343–1352.
37. Geng, Y.; Dalhaimer, P.; Cai, S.; Tsai, R.; Tewari, M.; Minko, T.; Discher, D. E. Shape Effects of Filaments *versus* Spherical Particles in Flow and Drug Delivery. *Nat. Nanotechnol.* **2007**, *2*, 249–255.
38. Gilroy, J. B.; Gädt, T.; Whittell, G. R.; Chabanne, L.; Mitchels, J. M.; Richardson, R. M.; Winnik, M. A.; Manners, I. Monodisperse Cylindrical Micelles by Crystallization-Driven Living Self-Assembly. *Nat. Chem.* **2010**, *2*, 566–570.
39. Schmelz, J.; Schedl, A. E.; Steinlein, C.; Manners, I.; Schmalz, H. Length Control and Block-Type Architectures in Worm-Like Micelles with Polyethylene Cores. *J. Am. Chem. Soc.* **2012**, *134*, 14217–14225.
40. Kaminskas, L. M.; Boyd, B. J.; Porter, C. J. H. Dendrimer Pharmacokinetics: The Effect of Size, Structure and Surface Characteristics on ADME Properties. *Nanomedicine* **2011**, *6*, 1063–1084.
41. Soto-Cantu, E.; Lokitz, B. S.; Hinestrosa, J. P.; Deodhar, C.; Messman, J. M.; Ankner, J. F.; Kilbey Ii, S. M. Versatility of Alkyne-Modified Poly(Glycidyl Methacrylate) Layers for Click Reactions. *Langmuir* **2011**, *27*, 5986–5996.
42. Benaglia, M.; Alberti, A.; Giorgini, L.; Magnoni, F.; Tozzi, S. Poly(Glycidyl Methacrylate): A Highly Versatile Polymeric Building Block for Post-Polymerization Modifications. *Polym. Chem.* **2013**, *4*, 124–132.
43. Müllner, M.; Lunkenbein, T.; Breu, J.; Caruso, F.; Müller, A. H. E. Template-Directed Synthesis of Silica Nanowires and Nanotubes from Cylindrical Core–Shell Polymer Brushes. *Chem. Mater.* **2012**, *24*, 1802–1810.
44. Müllner, M.; Lunkenbein, T.; Schieder, M.; Gröschel, A. H.; Miyajima, N.; Förtsch, M.; Breu, J.; Caruso, F.; Müller, A. H. E. Template-Directed Mild Synthesis of Anatase Hybrid Nanotubes within Cylindrical Core–Shell–Corona Polymer Brushes. *Macromolecules* **2012**, *45*, 6981–6988.
45. Geng, Y.; Discher, D. E. Hydrolytic Degradation of Poly(Ethylene Oxide)-Block-Polycaprolactone Worm Micelles. *J. Am. Chem. Soc.* **2005**, *127*, 12780–12781.
46. Yu-Su, S. Y.; Sheiko, S. S.; Lee, H.-i.; Jakubowski, W.; Nese, A.; Matyjaszewski, K.; Anokhin, D.; Ivanov, D. A. Crystallization of Molecular Brushes with Block Copolymer Side Chains. *Macromolecules* **2009**, *42*, 9008–9017.
47. Lee, H.-i.; Jakubowski, W.; Matyjaszewski, K.; Yu, S.; Sheiko, S. S. Cylindrical Core–Shell Brushes Prepared by a Combination of ROP and ATRP. *Macromolecules* **2006**, *39*, 4983–4989.
48. Saba, T. M. Physiology and Physiopathology of the Reticuloendothelial System. *Arch. Int. Med.* **1970**, *126*, 1031–1052.
49. Moghimi, S. M.; Porter, C. J. H.; Muir, I. S.; Illum, L.; Davis, S. S. Non-Phagocytic Uptake of Intravenously Injected Microspheres in Rat Spleen: Influence of Particle Size and Hydrophilic Coating. *Biochem. Biophys. Res. Commun.* **1991**, *177*, 861–866.
50. Elsabahy, M.; Wooley, K. L. Design of Polymeric Nanoparticles for Biomedical Delivery Applications. *Chem. Soc. Rev.* **2012**, *41*, 2545–2561.
51. Johnston, A. P. R.; Such, G. K.; Ng, S. L.; Caruso, F. Challenges Facing Colloidal Delivery Systems: From Synthesis to the Clinic. *Curr. Opin. Colloid Interface Sci.* **2011**, *16*, 171–181.
52. Liu, D.; Mori, A.; Huang, L. Role of Liposome Size and RES Blockade in Controlling Biodistribution and Tumor Uptake of GM1-Containing Liposomes. *Biochim. Biophys. Acta* **1992**, *1104*, 95–101.
53. Torchilin, V. Tumor Delivery of Macromolecular Drugs Based on the EPR Effect. *Adv. Drug Delivery Rev.* **2011**, *63*, 131–135.
54. Mori, H.; Wakisaka, O.; Hirao, A.; Nakahama, S. Protection and Polymerization of Functional Monomers, 23. Synthesis of Well-Defined Poly(2-Hydroxyethyl Methacrylate) by Means of Anionic Living Polymerization of Protected Monomers. *Macromol. Chem. Phys.* **1994**, *195*, 3213–3224.
55. Beers, K. L.; Boo, S.; Gaynor, S. G.; Matyjaszewski, K. Atom Transfer Radical Polymerization of 2-Hydroxyethyl Methacrylate. *Macromolecules* **1999**, *32*, 5772–5776.
56. Zheng, Z.; Müllner, M.; Ling, J.; Müller, A. H. E. Surface Interactions Surpass Carbon–Carbon Bond: Understanding and Control of the Scission Behavior of Core–Shell Polymer Brushes on Surfaces. *ACS Nano* **2013**, *7*, 2284–2291.
57. Boyd, B. J.; Kaminskas, L. M.; Karellas, P.; Krippner, G.; Lessene, R.; Porter, C. J. H. Cationic Poly-L-Lysine Dendrimers: Pharmacokinetics, Biodistribution, and Evidence for Metabolism and Bioresorption after Intravenous Administration to Rats. *Mol. Pharmaceutics* **2006**, *3*, 614–627.
58. Lyons, K. C.; Charman, W. N.; Miller, R.; Porter, C. J. H. Factors Limiting the Oral Bioavailability of *N*-Acetylglucosaminyl-*N*-Acetylmuramyl Dipeptide (GMDP) and Enhancement of Absorption in Rats by Delivery in a Water-in-Oil Microemulsion. *Int. J. Pharm.* **2000**, *199*, 17–28.